EDGE ARTICLE

Check for updates

The role of porphyrin peripheral substituents in determining the reactivities of ferrous nitrosyl species†

Sk Amanullah [ID] and Abhishek Dey [ID] *

Ferrous nitrosyl {FeNO}[7] species is an intermediate common to the catalytic cycles of Cd_1NiR and CcNiR, two heme-based nitrite reductases (NiR), and its reactivity varies dramatically in these enzymes. The former reduces NO_2^- to NO in the denitrification pathway while the latter reduces NO_2^- to NH_4^+ in a dissimilatory nitrite reduction. With very similar electron transfer partners and heme based active sites, the origin of this difference in reactivity has remained unexplained. Differences in the structure of the heme d_1 (Cd_1NiR), which bears electron-withdrawing groups and has saturated pyrroles, relative to heme c (CcNiR) are often invoked to explain these reactivities. A series of iron porphyrinoids, designed to model the electron-withdrawing peripheral substitution as well as the saturation present in heme d_1 in Cd_1NiR, and their NO adducts were synthesized and their properties were investigated. The data clearly show that the presence of electron-withdrawing groups (EWGs) and saturated pyrroles together in a synthetic porphyrinoid (FeDEsC) weakens the Fe–NO bond in {FeNO}[7] adducts along with decreasing the bond dissociation free energies ($BDFE_{NH}$) of the {FeHNO}[8] species. The EWG raises the E° of the {FeNO}[7/8] process, making the electron transfer (ET) facile, but decreases the pK_a of {FeNO}[8] species, making protonation (PT) difficult, while saturation has the opposite effect. The weakening of the Fe–NO bonding biases the {FeNO}[7] species of FeDEsC for NO dissociation, as in Cd_1NiR, which is otherwise set-up for a proton-coupled electron transfer (PCET) to form an {FeHNO}[8] species eventually leading to its further reduction to NH_4^+.

Introduction

Nitrite plays a vital role in the biochemical N-cycle.[1,2] Being generated from nitrate by the action of a molybdenum-containing nitrate reductase,[3] nitrite is consumed *via* several pathways which involve multiple heme and non-heme enzymes (Scheme 1A).[2] Assimilatory ammonification, catalyzed by sirohoheme containing nitrite reductase (CSNiR), and dissimilatory nitrite reduction, catalyzed by multi-*c* heme-containing nitrite reductase (CcNiR, Fig. 1A), lead to the formation of ammonium ion (NH_4^+) directly, without releasing any intermediate nitrogenous species.[4] Alternatively, denitrification involves the reduction of nitrite to nitric oxide (NO), catalyzed by heme cd_1 containing nitrite reductase (Cd_1NiR, Fig. 1B).[5] Further reduction of nitric oxide generates nitrous oxide,[6] which is eventually reduced further to dinitrogen.[7,8] Thus, CcNiR reduces nitrite to NH_4^+ without releasing any intermediate, and Cd_1NiR reduces

nitrite to release NO. Both of these enzymes have heme cofactors in their active site with a very similar distal environment and electron transfer partners (Fig. 1).
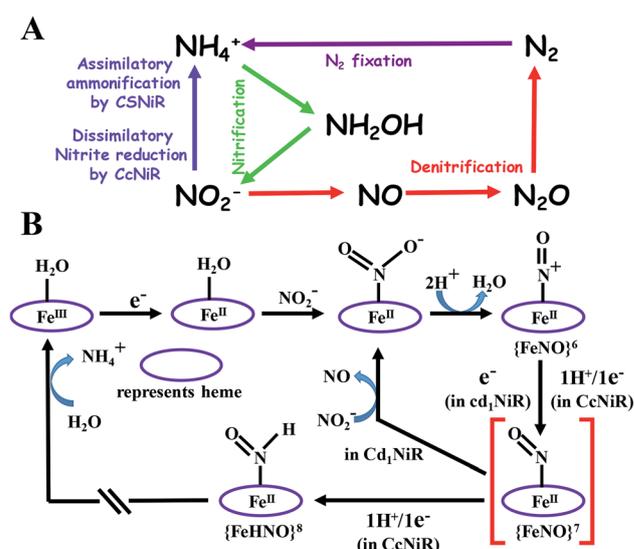
Scheme 1 (A) Selected components of the biochemical cycle of "N" and (B) proposed mechanistic pathways of nitrite reduction catalyzed by CcNiR and Cd_1NiR.[2]

School of Chemical Sciences, Indian Association for the Cultivation of Science, 2A & 2B Raja SC Mullick Road, Kolkata, India – 700032. E-mail: icad@iacs.res.in
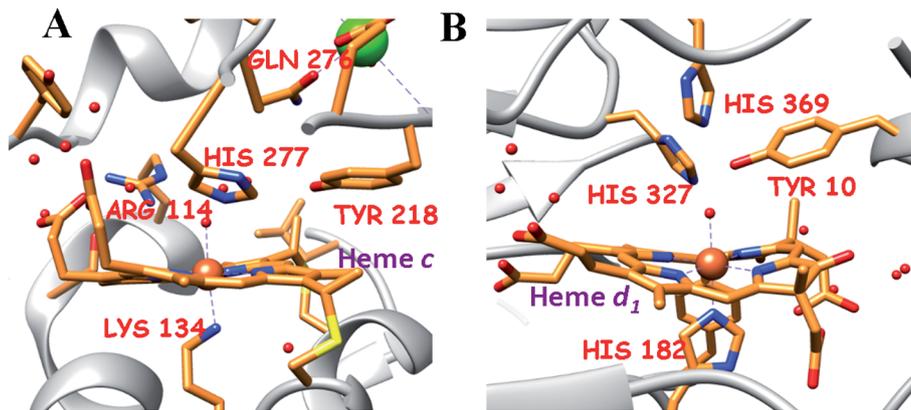
Fig. 1 The active site structure of the nitrite reductases at resting state; (A) CcNiR (pdb: 1FS7)[24] and (B) Cd₁NiR (pdb: 1NIR);[25] the figures are redrawn using the software package Chimera 1.12rc.

The proposed mechanistic pathways of both Cd_1NiR and CcNiR are quite similar (Scheme 1B).[2] The nitrite binds to the reduced ferrous iron center. With two protons from the distal residues, a molecule of water is released, forming a $\{FeNO\}^6$ intermediate (Enemark–Feltham notation).[5,9,10] The CcNiR avoids the formation of the dead-end intermediate, $\{FeNO\}^7$ through two consecutive proton-coupled electron transfer (PCET) to the $\{FeNO\}^6$ species, generating an $\{FeHNO\}^8$ intermediate,[11] which, on further reduction, leads to the generation of NH_4^+.[9] Alternatively, Cd_1NiR forms $\{FeNO\}^7$ through an electron transfer (ET) from cytochrome c, and releases NO with the concomitant binding of nitrite to the ferrous heme-d_1 and the cycle continues.[12–14] The different reactivity of $\{FeNO\}^7$ species compels investigating the difference in the active sites that controls the competition between the PCET process and NO release. A $\{FeNO\}^7$ adduct generally possesses a very strong Fe–NO bond with a $K_d \sim 10^{-9}$ and this displacement of NO by nitrite is rather unexpected.[15] Although the N–O stretch of the $\{FeNO\}^7$ species of CcNiR is not reported, the N–O stretch of Cd_1NiR is higher than that of other known heme proteins like hemoglobin and myoglobin.[16–18] We find a strong positive

correlation between the reported rate of NO dissociation and the corresponding N–O frequency (Fig. 2A). It suggests that the rate of NO dissociation is reflected by the strength of the Fe–NO bond, which is reflected in the N–O stretching vibration.[16–21] Similar correlation is also present between the N–O stretching frequency and the rate of NO displacement by pyridine in different synthetic meso-phenyl substituted Fe-porphyrins (Fig. 2B).[22] Iron-porphyrins bearing electron-withdrawing groups (EWGs), having higher N–O stretching frequency, release NO easier. Previous work from our group demonstrated that the iron-porphyrins bearing EWGs and/or saturated β-pyrrolic carbons form weaker iron-nitrosyls due to the competitive back-bonding between macrocycle π^* and NO π^*-orbitals from the filled Fe-d_π orbitals.[23]

CcNiR and Cd_1NiR possess basic 2nd sphere distal residues and primarily σ-donor histidine or lysine axial ligands and the same redox partner (cytochrome c). These residues assist in NO_2^- binding, proton translocation and are likely to affect the dissociation constants of NO_x ligands.[9,11,26,27] Another major distinction is the difference in the nitrite binding sites: heme c in CcNiR, and heme d_1 in Cd_1NiR (Fig. 1).[24,25] The major
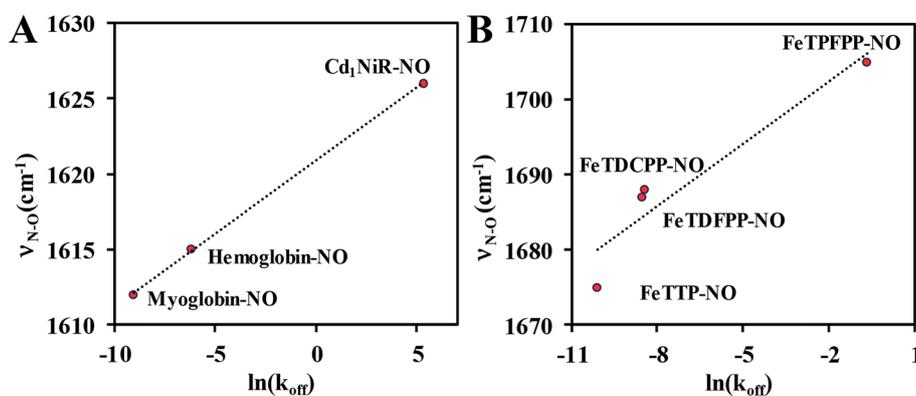

Fig. 2 Correlation between N–O stretching frequency[16–18] and rate of NO dissociation:[19–21] (A) in six-coordinate heme nitrosyls in enzyme systems; (B) in synthetic Fe-porphyrin nitrosyl complexes, TTP (p-tolyl), TDFPP (2,6-difluorophenyl), TDCPP (2,6-dichlorophenyl), TPFPP (pentafluorophenyl).
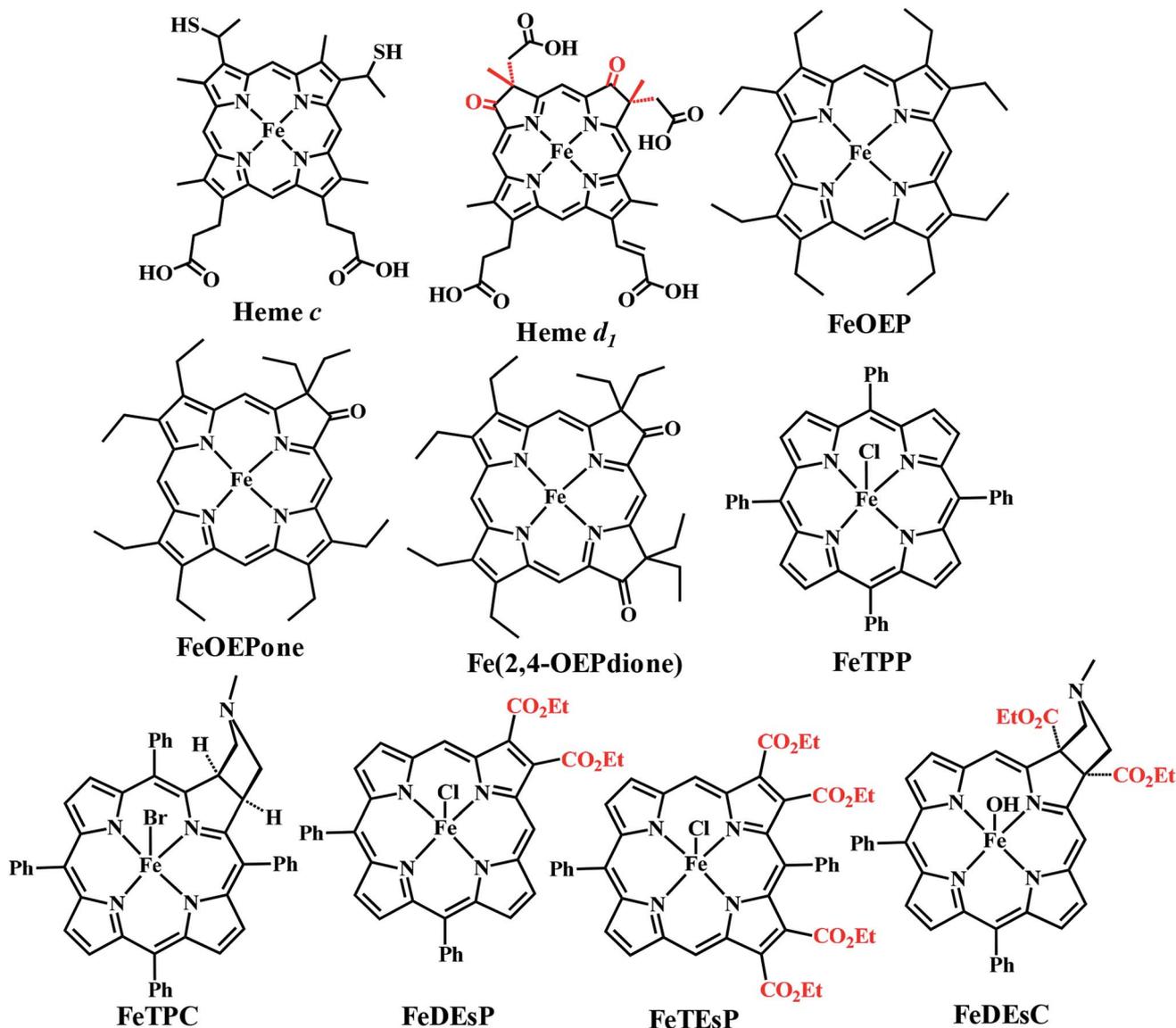
Fig. 3 Structure of the naturally occurring heme and synthetic Fe-porphyrinoids. FeOEP, FeOEPone, and Fe(2,4-OEPdione) were synthesized previously.[32,47,48]

difference in heme d_1, relative to heme c is the presence of two saturated β-pyrroles (*i.e.*, sp[3] hybridized peripheral carbons) along with two electron-withdrawing keto-groups (Fig. 3).[28,29] Therefore, their divergent reactivity may stem from differences in the structure of iron-porphyrinoid macrocycles. To evaluate this possibility, the electrochemistry of synthetic iron-porphyrin model complexes (FeTPP, FeOEP, FeOEPone and Fe(2,4-OEPdione), Fig. 3) and their nitrosyl adducts has been investigated by several groups.[30–39] Under coulometric conditions, nitrite could be reduced to ammonium ion by the synthetic complexes mediated by a hydroxylamine bound species.[40–43] The rate of the reaction was strongly directed by the macrocycle *i.e.*, FeOEP reacted faster than FeTPP and the reaction was very slow in the Fe(2,4-OEPdione) complex. The basicity of {FeNO}[8] species could potentially explain the difference in reactivity.[42] Alternatively, the greater Lewis acidity of {Fe(2,4-OEPdione)–NO}[7] (as suggested by the facile pyridine binding to the

Fe) was suggested to enhance the His-coordination with heme d_1 which might help the release of the *trans* NO.[33] These results herald the intrinsic nature of the macrocycle as a determinant of the different reactivity of the {FeNO}[7] species, *i.e.*, NO release *vs.* PCET. An {FeHNO}[8] species (converted after PCET to {FeNO}[7]) is quite reactive and so far could only be transiently observed in protected environments such as proteins,[44,45] or in bis-picket fence porphyrin[46] or in highly electron-rich FeOEP in the presence of weak acids such as substituted phenols.[41] Alternatively, under electrochemical conditions, {FeNO}[8] yields the parent {FeNO}[7] species and H$_2$.[43] It is important to understand the role of these peripheral modifications in the electronic structure and reactivity of these iron nitrosyls, to understand the different reactivities of the {FeNO}[7] species exhibited by these enzymes.

In this manuscript, a series of synthetic iron-porphyrins were developed for systematically varying their peripheral
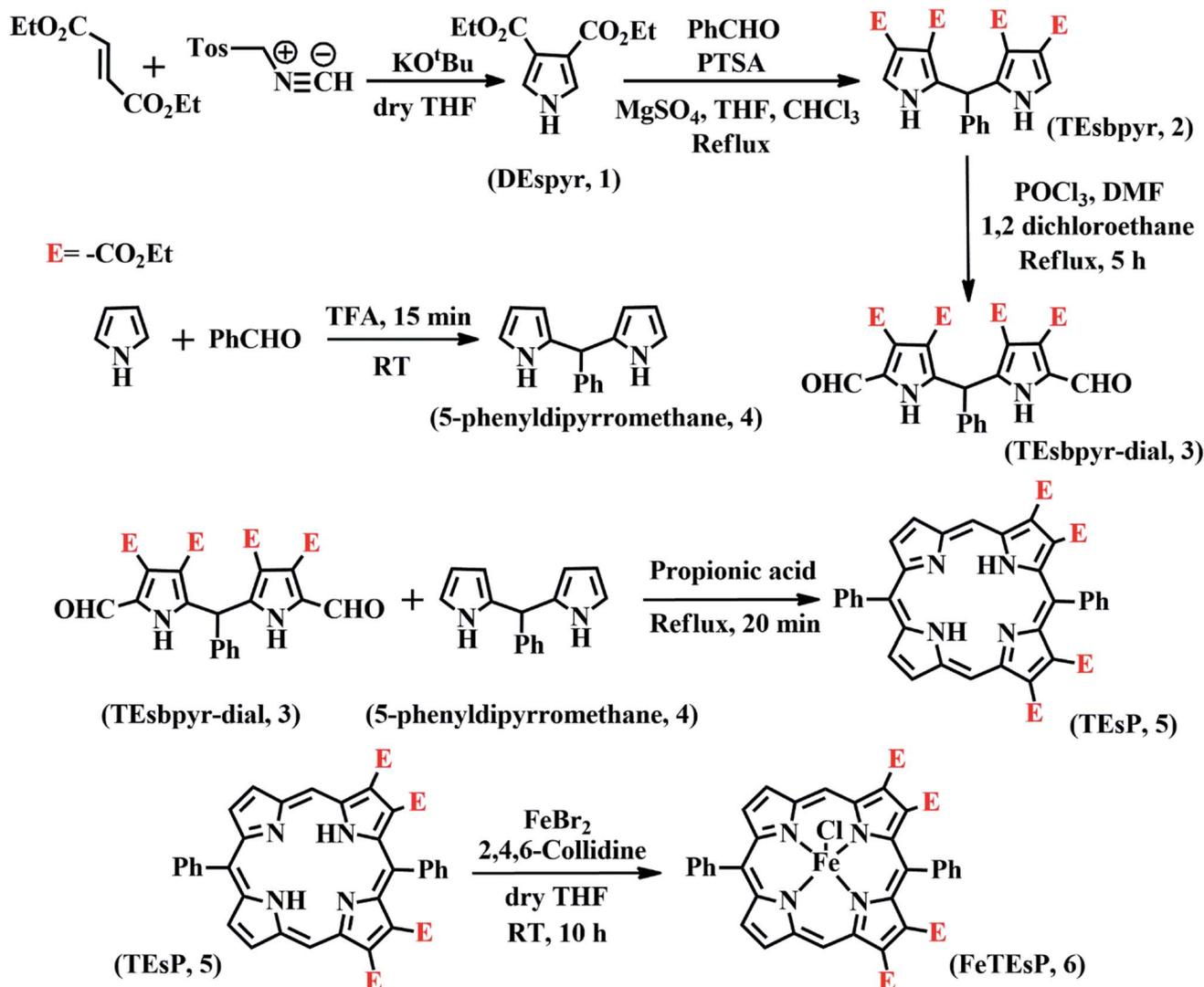
Scheme 2 Synthetic strategy of FeTEsP. In some cases, the −CO₂Et group is abbreviated as "E" for clarity in representation.

substituents. By introducing EWGs and/or saturation at the β-pyrrolic positions, we were able to decode the role of each substituent on the basic iron-porphyrin skeleton in the electronic structure and reactivity of their corresponding {FeNO}^{7} species. The electrochemical and spectroscopic data of their NO adducts and density functional theory (DFT) calculations help delineate the contribution of reduction potential and pK_a to the bond dissociation free energy (BDFE$_{NH}$) of the N–H bond in the {FeHNO}^{8} species. The results indicate a definitive role of EWG and saturation in tuning the Fe–NO bond strength, the reduction potential of {FeNO}^{7} and pK_a of {FeNO}^{8} species, which can likely explain the origin of differences in the reactivity of CcNiR and Cd₁NiR.

Results

Synthesis

The heme involved in the nitrite binding sites of CcNiR and Cd₁NiR is heme c and heme d_1, respectively. The major

difference between these is the presence of two electron-withdrawing-keto groups and two saturated β-pyrrolic carbons in heme d_1 (Fig. 3). To rationalize the effect of the EWG and/or saturation, a series of iron-porphyrinoids were synthesized (Fig. 3), namely, iron-tetraphenylporphyrin (FeTPP, fully unsaturated); iron-diesterporphyrin (FeDEsP, having two electron-withdrawing ester groups); iron-tetraesterporphyrin (FeTEsP, having four ester groups); iron-tetraphenylchlorin (FeTPC, having two saturated β-pyrrolic carbons) and iron-diesterchlorin (FeDEsC, having two ester groups and two saturated β-pyrrolic carbons). The EWGs were designed to qualitatively emulate the −I (inductive) effect of the keto-groups in heme d_1. FeTPP, FeTPC, FeDEsP, and FeDEsC complexes were synthesized following previously reported procedures.[23,49]

FeTEsP was synthesized to introduce four electron-withdrawing substitutions on the porphyrin ring. TEsP (5 in Scheme 2) was synthesized by the propionic acid condensation of two dipyrromethanes (Scheme 2), one of which (TEsbpyr-dial, 3 in Scheme 2) contained four ester groups (at the 3 and 4
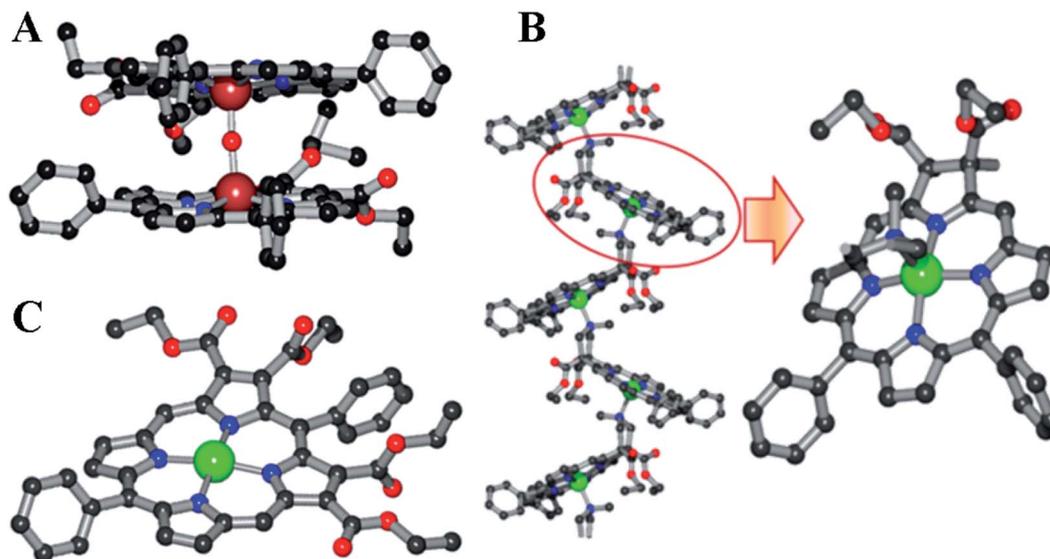
Fig. 4 Molecular structures of the crystals of (A) a μ-oxo dimer of FeDEsP; (B) ZnDEsC, and (C) ZnTEsP. Color code: C, black; Fe, brownish-red; Zn, green; N, blue; O, red. Hydrogen atoms are omitted for clarity.

positions of the respective pyrroles) as well as two aldehyde groups (at the 2 positions of the respective pyrroles) and the other half was 5-phenyldipyrromethane (4 in Scheme 2). Base induced cyclization of diethyl fumarate and *p*-toluenesulfonylmethylisocyanide (TosMIC) leads to the formation of a pyrrole bearing two ester groups (DEspyr, 1 in Scheme 2). The dipyrromethane of DEspyr (TEsbpyr, 2 in Scheme 2) was obtained by the condensation with benzaldehyde under harsh acidic conditions. A Vilsmeier–Haack reaction was performed upon TEsbpyr to obtain the corresponding dialdehyde, TEsbpyr-dial (3 in Scheme 2).

The other half, *i.e.*, the 5-phenyldipyrromethane (4 in Scheme 2), was prepared by the acid-catalyzed condensation of pyrrole and benzaldehyde following the Lindsey protocol.[50] Zinc and iron metalation was performed using established protocols.[49] The zinc complex of TEsP was characterized by single-crystal XRD. Needle-shaped purple crystals of ZnTEsP were grown from the diffusion of hexane into a chloroform solution of the complex (Fig. 4C). It crystallized in a triclinic symmetry with a centrosymmetric $P\bar{1}$ space group. Structural analysis revealed that it was a dimer, formed by the coordination of a free carbonyl "oxygen" atom with the zinc atom of another molecule. The structures of FeDEsP and ZnDEsC were reported before and are shown here for comparison (Fig. 4A and B). Further investigations were performed with the nitrosyl adducts of the iron-bound porphyrinoids.

Iron-nitrosyl reduction potentials

The cyclic voltammograms of the nitrosyl complexes of FeTPP, FeDEsP, FeTEsP, FeTPC, and FeDEsC showed an oxidation process at 0.20, 0.34, 0.38, −0.04 and 0.10 V, respectively, against the Fc⁺/Fc redox couple (Fig. 5). For FeTPC and FeDEsC, the process was clearly observed only under fast scan rates (Fig. S23B†). The process was irreversible at slow scan rates, indicating dissociation of the NO during oxidation. Note that

the CV of FeDEsC was performed under NO saturation condition to prevent NO loss from the complex. Past research from the Ryan and Kadish group established the nature of these redox events: the oxidation wave of porphyrin {FeNO}[7] leads to the formation of Fe^III–NO species, while in the case of chlorins, bacterio/iso-bacteriochlorins, and porphinone/porphinediones, the oxidation leads to the formation of Fe^II–NO species with the macrocycle-cation radical.[32,33,36,51] The {FeNO}[7/8] process was observed for FeTPP, FeDEsP, FeTEsP, FeTPC, and FeDEsC at −1.41, −1.24, −1.14, −1.51 and −1.42 V, respectively, *vs.* the Fc⁺/Fc redox couple (Fig. 5). The values obtained for FeTPP were consistent with previous reports.[38] The pre-wave observed in the
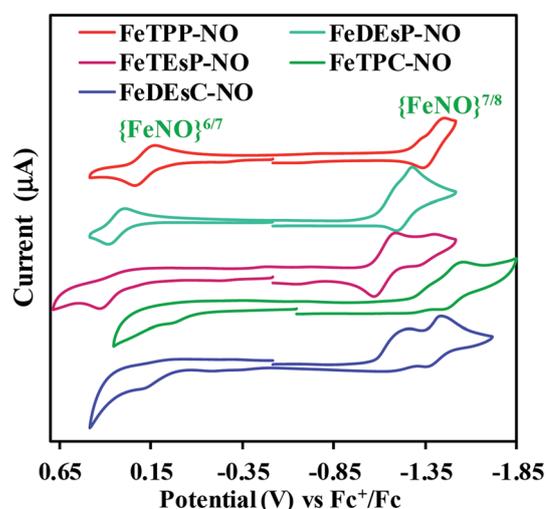

Fig. 5 Cyclic voltammograms of the complexes in dichloromethane at room temperature. Working electrode: glassy carbon; counter electrode: platinum; reference electrode: aqueous Ag/AgCl in 4 M KCl; supporting electrolyte: tetrabutylammonium hexafluorophosphate (100 mM); scan rate: 50 mV ps.

case of FeTPP (-1.32 V), FeDEsP (-1.17 V) and FeTPC (-1.38 V) might be due to ligand association, which disappeared at higher scan rates (Fig. S23A†) as reported by the Kadish group earlier.[38,52] In the case of FeDEsC, the irreversible pre-wave at $\sim$ -1.22 V vs. the Fc$^+$/Fc redox couple was likely due to the direct electrochemical NO reduction[53] (NO saturated solution), as observed by the Kadish group during the reduction of Fe^{II}–TPP–NO and Fe^{II}–OEP–NO, in the presence of excess NO gas in the medium.[38]

A clear trend was observed in both the oxidation and reduction process of the {FeNO}^{7} species for the series of iron porphyrinoids used here. With an increase in the number of EWGs attached to the β-pyrroles relative to FeTPP–NO, both {FeNO}$^{6/7}$ and {FeNO}$^{7/8}$ couples shifted to higher potential (i.e., for FeDEsP–NO and FeTEsP–NO in Fig. 5). Alternatively, saturating one of the pyrroles of FeTPP–NO, i.e., in the case of FeTPC–NO, both the reduction couples shifted to lower potentials. The FeDEsC–NO complex, having both EWGs as well as saturated pyrrole centers, had both the reduction potentials

almost similar to those of FeTPP–NO. This implied that the EWG and saturation had opposite effects on the electronic structure of the Fe–NO unit.

Fe–NO bond strength

The FTIR data of the five-coordinate {FeNO}^{7} complexes of FeTPP, FeDEsP, FeTEsP, FeTPC, and FeDEsC showed the N–O stretch at 1676, 1686, 1688, 1680 and 1691 cm^{-1}, respectively (Fig. 6). The data showed that when two EWGs were introduced (FeDEsP), the N–O vibration (str.) shifted to 1686 cm^{-1} from 1676 cm^{-1} in FeTPP. Further addition of EWGs (FeTEsP), shifted the N–O vibration (str.) up to 1688 cm^{-1}. Such high N–O stretching frequencies had only been reported for {FeNO}^{7} species of octa-halogenated porphyrins and reflect poor back-bonding between the occupied iron and unoccupied NO π*-orbitals.[22,54] The saturation of the pyrrole, by itself, exerted little effect on Fe–NO bonding as indicated by the N–O stretching frequency of {FeTPC–NO}^{7} at 1680 cm^{-1} which was very similar to that of {FeTPP–NO}^{7}. But saturation along with EWGs caused
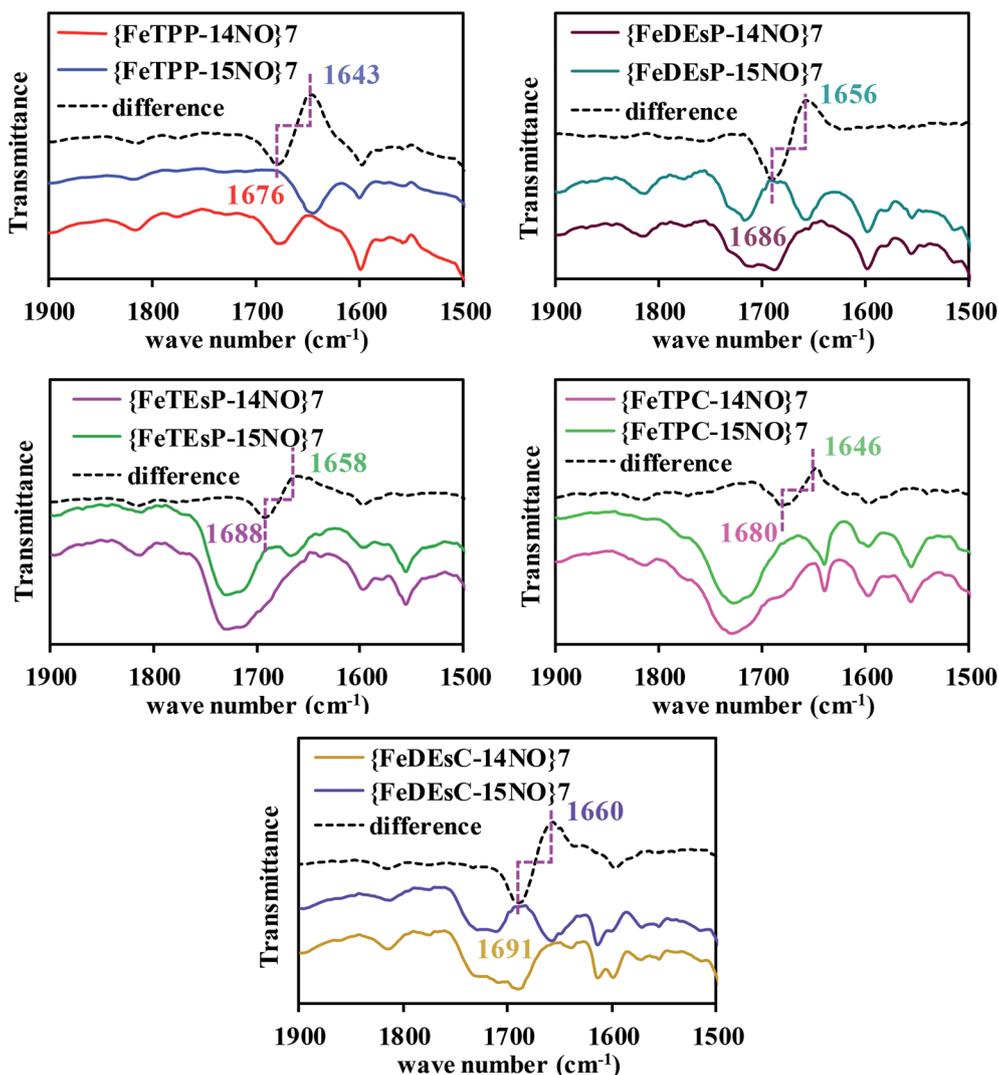

Fig. 6 FTIR data of the {FeNO}^{7} adducts in dichloromethane at room temperature.

a substantial weakening of the NO adduct, as indicated by the N–O stretch of {FeDEsC–NO}[7] at 1691 cm^{-1}, relative to {FeTPP–NO}[7] at 1676 cm^{-1}. The Fe–N stretch of the {FeNO}[7] species of FeTPP–NO reproduced the previously reported value. However, despite several attempts with resonance Raman the Fe–N stretching frequencies could not be obtained for the other compounds studied (Fig. S24A†).[43] The strength of the Fe–NO bond in the {FeNO}[7] adducts was strongly dictated by both σ-bonding and π-back-bonding.[55–58] As reported recently, the presence of electron-withdrawing substitutions on the porphyrin lowers the energy of the porphyrin π*-orbitals. This results in competitive back-bonding from the filled d$_\pi$ orbitals of Fe between porphyrin π* and NO π*-orbitals, which eventually weakens the NO adducts.[23] Saturation by itself had a minor effect on the back-bonding. However, saturation along with two EWGs had an enhanced effect on the weakening of the NO-adduct.

Qualitatively, a similar trend was observed for N-methylimidazole bound six-coordinate {FeNO}[7] species where the N–O stretching vibrations for FeTPP, FeDEsP, FeTEsP, FeTPC, and FeDEsC were observed at 1626 cm^{-1}, 1641 cm^{-1}, 1646 cm^{-1}, 1635 cm^{-1} and 1633 cm^{-1}, respectively (Fig. S25A†). Therefore, an axial, primarily σ donor, nitrogenous ligand has a very limited effect on the electronic structure of these {FeNO}[7] complexes. Note that the N–O stretching of the {FeNO}[7] species in Cd$_1$NiR was 1626 cm^{-1} with heme d_1, relative to 1612 cm^{-1} in myoglobin with heme b (which neither has an EWG nor saturation).[16–18] The higher N–O stretching frequency in Cd$_1$NiR (by 14 cm^{-1}) was indicative of a weaker Fe–NO bonding. And it was associated with a ~10^6 fold enhancement in NO dissociation rate from the {FeNO}[7] intermediate (Fig. 2).[13,19–21,59] The 15 cm^{-1} upshifting of the N–O vibration observed here between FeDEsC and FeTPP mirrored the 14 cm^{-1} shift observed between Cd$_1$NiR and myoglobin suggesting a weakening of the Fe–NO bond, raising the possibility of ligands like NO$_2^-$ displacing the bound NO.

The displacement of the bound NO from the N-methyl-imidazole bound six-coordinated {FeNO}[7] species by NO$_2^-$ was investigated using absorption spectroscopy (see the ESI, Section 8†). The K_d for the process (Fe^{II}–NO + NO$_2^-$ ⇌ Fe^{II}–NO$_2^-$ + NO) was determined to be 0.09 for FeTPP and 0.46 for FeDEsC (Table 1). The higher K_d for FeDEsC, relative to FeTPP, translated to a ΔG difference of ~1 kcal mol^{-1} and correlated very well with its stronger N–O stretching frequency and demonstrated clearly

how the EWG and saturation of the porphyrin ring aid the displacement of NO by NO$_2^-$, as proposed for Cd$_1$NiR. A similar effect was observed on the displacement rate of NO by pyridine in {FeNO}[7] complexes in a series of iron porphyrins, where the octa-halogenated derivative of TPP was ~10^6 times faster than that of FeTPP.[22]

Spectroelectrochemistry was used to access the N–O vibrations of the {FeNO}[6] and {FeNO}[8] species (Table 1, Fig. S26–S28†). The N–O vibrations for the six-coordinate {FeNO}[6] for FeTPP, FeDEsP, and FeTEsP were obtained at 1914 cm^{-1}, 1923 cm^{-1}, and 1927 cm^{-1}, respectively (Fig. S27†). The higher N–O vibration for the porphyrins containing EWGs relative to FeTPP mirrored the trend observed for the corresponding {FeNO}[7] species. The N–O vibrations for both five and six-coordinate {FeNO}[6] species of FeTPC and FeDEsC could not be obtained, which was consistent with the irreversible CV observed for these species indicating that the {FeNO}[6] species dissociate within the time scale of the experiment (Fig. S23B and S27†). The inability to identify five-coordinate {FeNO}[6] species of FeDEsP and FeTEsP again suggested the formation of a labile {FeNO}[6] adduct. The N–O vibrations for the {FeNO}[8] species could be observed for FeTEsP and FeDEsC at 1550 cm^{-1} and 1537 cm^{-1}, respectively (Fig. S28 and Table S2†). The values obtained were consistent with the previously reported values for the five-coordinate {FeNO}[8] porphyrins.[54,60,61] Note that the frequencies were much higher than the value reported for FeTPP at 1496 cm^{-1}.[43] Here, too, the inclusion of the EWG and saturation together leads to a substantial increase in the N–O vibration indicating a weakening of the Fe–NO bonding. Thus, the FTIR data for the {FeNO}[6], {FeNO}[7], and {FeNO}[8] species all showed that the inclusion of EWG and saturation at the periphery of the porphyrin macrocycle substantially weakened the Fe–NO bonding.

A plot of the experimentally observed N–O vibrations (Table 1) with ln(K_d) for the series of complexes investigated here showed a reasonably linear correlation (Fig. 7) in line with the linear correlation observed between ν(N–O) and ln(k_{off}) (Fig. 2). Thus, the electronic structure responsible for the correlation in the enzyme active site was captured in the series of porphyrins used here – primarily the competitive back-bonding between porphyrin π* and NO π*-orbitals adding credence to the use of the electron-withdrawing

Table 1 Properties of {FeNO}[6//7/8] species for the synthetic porphyrins

	{FeNO}[6] $\nu_{N-O}{}^a$ 5C (6C)	⇔ $E^{\circ,b}$	{FeNO}[7] ν_{N-O} 5C (6C)	⇔ E°	{FeNO}[8] ν_{N-O} 5C (6C)	$K_d{}^e$
FeTPP–NO	1844 (1914)	0.20	1676 (1626)	−1.41	1496 (ref. 43)	0.09 ± 0.05
FeDEsP–NO	^{c} (1923)	0.34	1686 (1641)	−1.24	^{c}	0.20 ± 0.04
FeTEsP–NO	^{c} (1927)	0.38	1688 (1646)	−1.14	1550	0.23 ± 0.02
FeTPC–NO	^{d}	−0.04^d	1680 (1635)	−1.51	^{c}	0.13 ± 0.04
FeDEsC–NO	^{d}	0.10^d	1691 (1633)	−1.42	1537	0.46 ± 0.04

^{a} Stretching frequency in cm^{-1}. ^{b} Potentials are reported vs. Fc$^+$/Fc in dichloromethane. ^{c} Not observed. ^{d} Irreversible cathodic waves. ^{e} Fe^{II}–NO + NO$_2^-$ ⇌ Fe^{II}–NO$_2^-$ + NO.
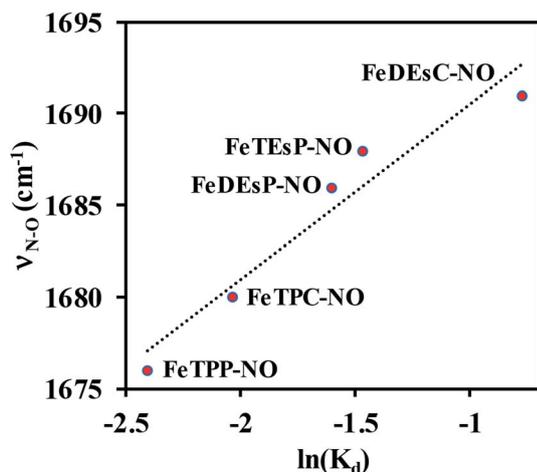
Fig. 7 Correlation between experimentally measured N–O stretching frequency and NO dissociation constant.

Table 2 Values of pK_a, $E°$, and $BDFE_{NH}$ relative to FeDEsC–NO

Complexes	ΔpK_a	$\Delta E°$ (mV)	$\Delta BDFE_{NH}$ (kcal mol^{-1})
FeTPP–NO	1.57	10	2.38
FeDEsP–NO	−0.32	180	3.71
FeTEsP–NO	−3.12	280	2.18
FeTPC–NO	1.92	−90	0.56
FeDEsC–NO	—	—	—
FeOEP–NO	5.36	−70	5.73
FeOEPone–NO	0.91	140	4.47
Fe(2,4-OEPdione)–NO	−1.76	260	3.58

–COOEt group to mimic the keto-group in heme d_1. The K_d was larger for {Fe–NO}^{7} species with higher ν(N–O) frequency. The stronger back-bonding with the porphyrin π^* will reduce back-bonding to the NO π^* thus tuning its pK_a. It is conceivable that this will affect the thermodynamics of the PCET to {FeNO}^{7} to form {FeHNO}^{8}.

PCET to {FeNO}^{7}

The {FeNO}^{7} species of CcNiR, with heme c, accepts 1H$^+$/1e$^-$ to form {FeHNO}^{8} on its way to form NH$_4$$^+$ without releasing any intermediate species and does not dissociate NO.[9] The lower N–O stretch in {FeNO}^{7} of heme c (1651–1671 cm^{-1}),[62] in general, was suggestive of a weak NO dissociation in CcNiR. But, for a facile PCET, the BDFE of the N–H bond in {FeNHO}^{8} should be high as well.[63] The BDFE of the N–H bond in {FeHNO}^{8} species can be calculated using the following equation:[64]

$$BDFE_{NH} = 1.37 pK_a + 23.06 E° + C$$

where the pK_a was that of {FeNO}^{8} species, which was calculated from the change in Gibb's free energy, $\Delta G°$ of the protonation equilibrium between {FeNO}^{8} and {FeHNO}^{8}. $E°$ represents the one-electron reduction potential of the {FeNO}$^{7/8}$ redox process, which was directly obtained from the cyclic voltammogram. C is a constant which depends on the solvent.[64] The pK_a of the {FeNO}^{7} species was difficult to determine as the protonation leads to an irreversible reaction.[42] Thus, the $\Delta G°$ of protonation was computed using DFT calculations. The $BDFE_{NH}$ values estimated using these were normalized relative to FeDEsC–NO which was set at 0 kcal mol^{-1} (Table 2). These calculations indicated that the protonation of {FeNO}^{8} species gradually became less favorable from FeOEP to FeOEPone to Fe(2,4-OEPdione). It was consistent with the previously reported trend for nitrite reduction to ammonia, using moderately strong acids like phenols, under controlled potential electrolysis, i.e., the rate of the reaction: FeOEP > FeOEPone > Fe(2,4-OEPdione),

where the protonation of {FeNO}^{8} species was proposed to be the rate-limiting step.[42]

Comparing the $\Delta G°$ for PCET to the {FeNO}^{7} species of FeDEsC–NO and FeDEsP–NO (without saturated pyrroles), the major contribution to the difference was derived from the $E°$ of the {FeNO}$^{7/8}$ redox process. $E°$ was increased by ~180 mV in FeDEsP–NO, making the reduction more facile. As a result, the $BDFE_{NH}$ of {FeHNO}^{8} species of FeDEsP–NO was increased by ~3.71 kcal mol^{-1}, relative to FeDEsC–NO, suggesting that the {FeNO}^{7} species of FeDEsP–NO should be more prone to undergo PCET reaction than FeDEsC–NO. Gratifyingly, during the electrochemical reduction of FeDEsP–NO, it generated N$_2$O in the presence of methanol as the proton source. This was evidenced by the growth of a vibrational band at 2224 cm^{-1} as a cathodic potential was applied (Fig. 8A), which shifted to 2154 cm^{-1} when ^{15}NO was used (Fig. 8B). The formation of N$_2$O from NO can be mediated by {FeHNO}^{8} which is difficult to characterize under electrochemical conditions.[65] Alternatively, when {FeDEsP–NO}^{7} was reduced chemically by cobaltocene in the presence of methanol and PPh$_3$, it readily generated Ph$_3$P= O and Ph$_3$P=NH (see the ESI, Section 10, Fig. S33–S35†), suggesting the generation of HNO in the solution. This can only happen if the reaction proceeds through the PCET process forming a {FeHNO}^{8} species.[66] Note that these results do not imply that FeDEsP mirrored the reactivity of CcNiR because CcNiR does not release any HNO, it generates NH$_4$$^+$ via {FeHNO}^{8} without releasing HNO or N$_2$O. The fact that FeDEsP– NO could produce HNO from a weak proton donor while the NO could be displaced by NO$_2$$^-$ in FeDEsC–NO suggested that the electronic structure of the porphyrin ring resulting from the EWG and saturation can discriminate NO release vs. PCET to a {FeNO}^{7} species under physiological conditions.

Discussion

It has been proposed that CcNiR undergoes two consecutive PCET reactions on the {FeNO}^{6} intermediate. The first PCET forms a {FeNO}^{7} species (with protonation of Arg$_{114}$ residue) which subsequently generates {FeHNO}^{8} species through another PCET process, releasing only a trace amount of the {FeNO}^{7} intermediate.[11,67] In contrast, Cd$_1$NiR undergoes an electron transfer (ET) from cytochrome c, forming the {FeNO}^{7} intermediate, which releases NO rapidly (k_{off} ~ 200 s^{-1}).[13,19] There is an extensive debate on whether the NO is released from
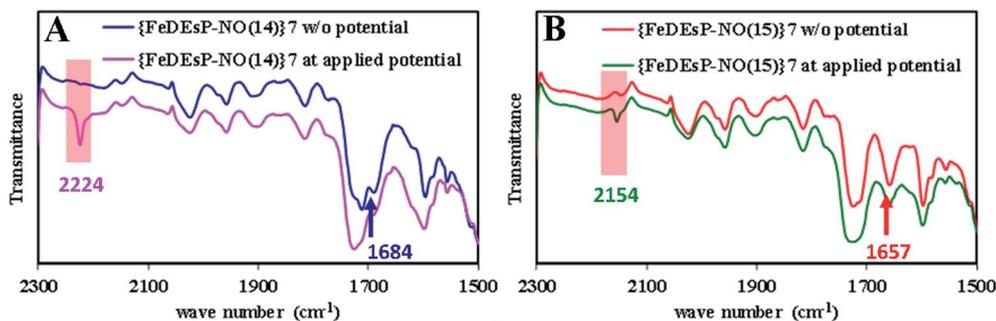
Fig. 8 Formation of N₂O during the electrolysis of {FeDEsP–NO}^{7} at −1.31 V (vs. Fc$^+$/Fc). On applying potential, N₂O is generated ($\nu_{N-O\,(14/15)}$: 2224/2154 cm^{-1}), with the expense of {FeDEsP–NO}^{7} peaks ($\nu_{N-O\,(14/15)}$: 1684/1657 cm^{-1}): (A) in the presence of ^{14}NO and (B) in the presence of ^{15}NO.

the ferric state or the ferrous state of the NO adduct.[1,68] Recent data suggest that it is likely that NO is released from the ferrous, {FeNO}^{7} state.[2,13,59] The fast release of NO from the {FeNO}^{7} intermediate may be attributed to a weak Fe–NO bonding in the ferrous nitrosyl adduct formed. The higher N–O stretching frequencies in the {FeNO}^{n} (n = 6, 7, and 8) species of FeTEsP and FeDEsC suggested weak Fe–NO bonding, i.e., four electron-withdrawing ester groups or two ester groups with two saturated carbon centers had an almost similar effect. Thus, heme d_1, which had two EW-keto groups and two saturated pyrrolic carbons, was likely to have a weaker Fe–NO bond relative to heme c, which has neither. A weaker Fe–NO in FeDEsC is associated with a large K_d for NO$_2^-$ replacement relative to FeTPP consistent with the strong linear correlation between ν_{N-O} and K_d observed for both enzymatic and synthetic systems. Similarly, a weaker Fe–NO in the heme d_1 active site of Cd$_1$NiR, evident from a higher ν_{N-O}, should result in higher NO (product) K_d, relative to NO$_2^-$ (substrate). It might be envisaged that due to the ruffled nature of the isobacteriochlorin ring in heme d_1, they form weak {FeNO}^{7} species. But calculations of the ruffling parameters[69] suggested that maximum ruffling was present in {FeTPC–NO}^{7} species, which possess a chlorin ring (see the ESI, Section 9†), and had a relatively strong Fe–NO bond.

The ΔG° for PCET to the {FeHNO}^{8}, the competing reaction to NO release, was affected by both E° and pK_a of the {FeNO}^{7} species. Between FeDEsC–NO and FeTPC–NO, where the latter was devoid of EWGs, the pK_a of {FeNO}^{8} species increased by 1.92 units (Table 2), but it lowered the E° of the {FeNO}$^{7/8}$ redox process by ∼90 mV (Table 2), making the PCET to the {FeNO}^{7} species of FeTPC–NO slightly favorable, relative to FeDEsC–NO. By omitting both saturation and EWGs (FeTPP–NO), the E° decreased while the pK_a of {FeNO}^{8} species increased which resulted in higher BDFE$_{NH}$ of the {FeHNO}^{8} species but it was not as high as that of FeDEsP–NO. In the case of FeTEsP–NO, where the saturation was absent but two more EWGs were present (relative to FeDEsC–NO), the E° increased by ∼280 mV but the pK_a of {FeNO}^{8} species becomes too low to be protonated, resulting in BDFE$_{NH}$ being lower than that of FeTPP–NO. Therefore, for a facile PCET, there needs to be a balance between E° and pK_a, which was attained here in FeDEsP–NO. This model was equally applicable to the FeOEP system, where

the high BDFE$_{NH}$ was due to the greater pK_a of the {FeNO}^{8} species. Introducing EW-keto groups increased the E° but at the expense of the pK_a of {FeNO}^{8} species (Table 2), resulting in a gradual decrease in BDFE$_{NH}$. However, it should also be noted that {FeHNO}^{8} species is not very stable due to the disproportionation of the Fe–HNO unit. The {FeHNO}^{8} species could only be stabilized either with steric protection (bis-picket fence porphyrin[46] or globin chain in hemoglobin[44,45]) or in a highly electron-rich porphyrin like FeOEP ($\nu_{NO/\{FeNO\}^7}$ = 1665 cm^{-1}).[41,70–72] Hence, it is not surprising that {FeHNO}^{8} species in electron-deficient octabromo[tetrakis(penta-fluorophenyl)]porphyrin, Fe(TFPPBr$_8$) (NO) ($\nu_{NO/\{FeNO\}^7}$ = 1726 cm^{-1})[54] could not be isolated. The weak BDFE$_{NH}$ and weaker {FeNO}^{7} adduct likely bias the FeDEsC (which have two EWGs along with two saturated pyrrolic carbons, like heme d_1 in the active site of Cd$_1$NiR) for NO dissociation. In contrast, stronger BDFE$_{NH}$ driven by a favourable balance between pK_a (due to better back-bonding to the NO π*-orbitals) and E° is responsible for facile PCET to {FeNO}^{7} to produce {FeHNO}^{8} which is necessary to eventually release NH$_4^+$ in CcNiR.

Conclusion

In summary, the results on structural variants of iron-porphyrins suggested that Cd$_1$NiR does not proceed with the PCET process to form {FeHNO}^{8} intermediate, due to its lower BDFE$_{NH}$ arising from the weaker back-donation from heme d_1 where the EWGs and sp^3 peripheral carbons enhance competitive back-bonding from the iron to the porphyrinoid π* and NO π*-orbitals. The weaker back-bonding to the bound NO results in a weaker Fe–NO bond and hence, it releases NO. In CcNiR, on the other hand, heme c has greater back-bonding to the NO from iron, which strengthens the Fe–NO bond and tunes the pK_a allowing PCET to occur to form {FeHNO}^{8} species, which is crucial for the further reactions to release NH$_4^+$.

Experimental details

Materials

All reagents were of the highest grade commercially available. Iodine, trifluoroacetic acid (TFA), 2,3-dichloro-5,6-dicyano-1,4-

benzoquinone (DDQ), ethanol, aqueous ammonia solution, ceric ammonium nitrate (CAN), sarcosine, potassium *tert*-butoxide, benzaldehyde, magnesium sulphate, *p*-toluenesulphonic acid (PTSA), *p*-toluenesulfonylmethyl isocyanide (TosMIC), phosphorus oxychloride ($POCl_3$), dichloroethane (DCE), and propionic acid were purchased from Spectrochem Ltd. Diethyl ether, tetrahydrofuran (THF), acetonitrile, dichloromethane, and toluene were purchased from RANKEM Ltd. Para-formaldehyde, anhydrous ferrous bromide ($FeBr_2$), 2,4,6-collidine, and tetrabutylammonium hexafluorophosphate ($TBAPF_6$) were purchased from Sigma-Aldrich chemical company. Na_2SO_4 and zinc acetate were purchased from MERCK and used without any further purification. Unless otherwise mentioned all reactions were performed at room temperature. Column chromatography was performed with silica gel (mesh size: 60–100, 100–200 and 230–400) and neutral alumina, preparative TLC was performed with silica gel GF-254 ($\sim$13% $CaSO_4$, $0.5H_2O$ binders with a fluorescent indicator). These were purchased from SRL Pvt. Ltd. THF was dried using K-metal in the presence of benzophenone until the colour of benzophenone turned intense bluish-green. Toluene was dried using Na-metal in the presence of benzophenone until the colour of benzophenone turned intense blue. MeOH was first dried like toluene using sodium after that it was distilled from Mg-cake. DCM and chloroform were distilled with both anhydrous $CaCl_2$ followed by CaH_2.

Instrumentation

All electrochemical experiments were performed using CH Instruments (model CHI700E and CHI710D Electrochemical Analyzer). The biopotentiostat, and reference electrode (standard single-junction silver/silver chloride filled with 4 M KCl with AgCl solution) were purchased from CH Instruments. The absorption spectra were measured in the SHIMADZU spectrograph (UV-2100). The aerobic and anaerobic cuvettes were purchased from Starna Scientific. The FT-IR data were measured on the Shimadzu FTIR 8400S instrument. The CaF_2 windows for IR spectroscopy were purchased from Sigma Aldrich. The anaerobic setup for IR spectroscopy was purchased from PerkinElmer. The optically transparent thin-layer electrochemical cell (OTTLE) was purchased from the University of Reading for spectroelectrochemistry. All the NMR spectra were recorded on a Bruker DPX-300, Bruker DPX-400 or DPX-500 spectrometer at room temperature. The mass spectra were recorded using the QTOF Micro YA263 instrument. Resonance Raman data were collected using a Trivista 555 spectrograph (Princeton Instruments) and using 413.1 nm excitation from a Kr^+ laser (Coherent, Sabre Innova SBRC-DBW-K). The X-band EPR spectra were recorded on a JEOL instrument. X-ray single-crystal data were collected at 120 K using radiation on a SMART APEX diffractometer equipped with a CCD detector. Data collection, data reduction, and structure solution refinements were carried out using the software package APEXIII. The structure was solved by the direct method and refined in a routine manner. The non-hydrogen atoms were treated anisotropically. All the

hydrogen atoms were located on a difference Fourier map and refined.

Electrochemical measurements

Since $\{FeNO\}^8$ readily reacts with a trace amount of water present in the solvents,[43] every solvent used in electrochemical measurements was first dried following the aforementioned protocol. After that, they were super-dried with activated 4 Å molecular sieves and kept inside the glove box for 1 week. Nitrosyl adducts of the five complexes (FeTPP, FeDEsP, FeTEsP, FeTPC, and FeDEsC) were considered for electrochemical analysis. All CV data were collected under anaerobic conditions in a custom made electrochemical cell. 6 ml of NO-complex (concentration: 1 mM) was taken in the presence of 100 mM $TBAPF_6$ as the supporting electrolyte. The glassy carbon electrode was taken as the working electrode, standard single-junction silver/silver chloride filled with 4 M KCl with AgCl solution as the reference electrode and a Pt electrode was taken as the counter electrode. Ferrocene (Fc) was used as an internal reference and the potential scale is normalized with respect to the potential of the Fc^+/Fc couple. The potential was swept starting from 0 V to a positive potential (oxidation) followed by negative potential (reduction), except for FeDEsC–NO, where sweeping positive potentials led to irreversible CV. Hence, for this, the potential was swept from 0 V to negative potential (reduction) followed by positive potential (oxidation).

NO complex preparation

Dry degassed NO gas was generated upon the dropwise addition of a deaerated saturated solution of sodium nitrite to the deaerated 6 M H_2SO_4. The gas was passed through two 4 N KOH solution bubblers followed by one concentrated H_2SO_4 solution. The solution of each complex was reduced by 0.5 equivalent Na_2S solution (in methanol) inside a glove box, sealed properly and kept out of the box. NO gas was purged through the samples (kept in an ice bath to reduce solution evaporation) for 5 min. The vials were tightly sealed and used for further investigations. NO complexes were also prepared using Ph_3-CSNO (as well as $Ph_3CS^{15}NO$), which were prepared through reported procedures.[73,74] To the reduced samples, 1 equivalent of Ph_3CSNO in THF/DCM (whichever required) was added. The vials were perfectly sealed and used for further investigations. The detailed characterization of the five and six-coordinated *N*-methylimidazole bound $\{FeNO\}^7$ adducts is given in the main text and the ESI (Fig. S24A–C, Table S1†).

FTIR data collection

DCM/THF solutions of the complexes were injected in the anaerobic FTIR setup or OTTLE cell and tightly sealed inside a glove box. The cell was removed from the box and data collected. Spectroelectrochemistry was performed using the OTTLE cell connected with the electrochemical analyzer. The sample solution contained 100 mM $TBAPF_6$ as the supporting electrolyte. The FTIR spectra were taken at different time intervals under electrolysis conditions.

UV-vis absorption data collection

All anaerobic data were collected taking the samples from the glove box in a tightly sealed anaerobic cuvette. The cuvette was removed from the box and data were collected. The background was corrected before the experiments, using an identical amount of solvent mixture.

Computational details

All calculations were performed at the IACS computer cluster using Gaussian 03 software.[75] BP86 functional reproduced better agreement with the experimental frequencies and hence further calculations were performed with that functional. A mixed basis set with 6-311g* on Fe and 6-31g* on C, O, N and H atoms were used for optimization.[76,77] For the final energy and ground-state calculations, a 6-311+g* basis set was used on all atoms. The solvent effect was corrected using the Polarizability Continuum Model (PCM).[78] For all complexes spin-unrestricted schemes have been adopted which distinguish between α and β-spin orbitals. Frequency calculations were performed using the basis set used for optimization, and no negative frequencies were found for the structures reported.

Synthesis details

The FeTPP, FeTPC, FeDEsP and FeDEsC complexes were synthesized following the reported procedures.[23] The synthetic procedure of FeTEsP is described below:

Diethyl 1*H*-pyrrole-3,4-dicarboxylate (DEspyr)

110 ml dry THF was added to potassium tertiary butoxide (15.57 g, 138.7 mmol) in a flask attached to a Schlenk line in a N_2 atmosphere. A solution of tosyl methyl isocyanide (Tos-MIC) (13.5 g, 69.4 mmol) and diethyl fumarate (10 ml, 69.4 mmol) in 60 ml dry THF was prepared and added dropwise to the flask kept in an ice water bath. Stirring was continued for 6 to 7 hours at room temperature. Then THF was evaporated and the reaction was quenched using saturated NH_4Cl solution. The mixture was worked up with ethyl acetate and dried over Na_2SO_4 and evaporated through a rotary evaporator. Purification was done by recrystallization from methanol. Crystals obtained were washed with cold ethyl acetate. ^1H NMR (CDCl$_3$): δ (ppm) 1.30 (t, 6H), 4.25 (q, 4H), 7.38 (d, 2H), 10.57 (bs, 1H). ^{13}C {^1H} NMR (CDCl$_3$): δ (ppm) 14.33, 60.26, 115.39, 126.59, 166.42. ESI-MS (positive ion mode, CH$_3$CN): m/z 234.05 (100%; [M + Na]$^+$), 212.09 (45%; [M + H]$^+$), 250.05 (30%; [M + K]$^+$).

Tetraethyl 2,2′-(phenylmethylene)bis(1*H*-pyrrole-3,4-dicarboxylate) (TEsbpyr)

p-Toluenesulphonic acid (0.89 g, 4.7 mmol) and MgSO$_4$ (0.23 g, 1.9 mmol) were taken in a flask. Benzaldehyde (194 μl, 1.9 mmol) was added to it in a N_2 atmosphere. The solid mixture was heated under vacuum until yellow colouration. Then THF (2 ml) was added and it was heated for 5 minutes. Then a solution of DEsPyr (1 g, 4.7 mmol) in dry CHCl$_3$ was added to it. The solution was refluxed for 5 hours. The reaction was quenched

using concentrated NaOH solution and was worked up with dichloromethane. The organic layer was dried over Na_2SO_4, evaporated through a rotary evaporator and was dissolved in a minimum amount of DCM and charged on a GF-254 silica gel preparative TLC plate and eluted with 30% ethyl acetate–hexane mixture. The product band was scratched off and extracted with ethyl acetate. ^1H NMR (CDCl$_3$): δ (ppm) 1.14 (t, 6H), 1.33 (t, 6H), 4.03 (q, 4H), 4.26 (q, 4H), 6.27 (s, 1H), 6.88 (d, 2H), 7.22 (m, 5H), 10.64 (bs, 2H), 1.26, 2.04, 4.12 (for EtOAc). ^{13}C {^1H} NMR (CDCl$_3$): δ (ppm) 13.75, 14.26, 40.51, 60.11, 61.08, 113.21–139.15, 164.01, 167.00. ESI-MS (positive ion mode, CH$_3$CN): m/z 533.35 (100%; [M + Na]$^+$), 549.34 (45%; [M + K]$^+$), 511.38 (35%; [M + H]$^+$).

Tetraethyl 5,5′-(phenylmethylene)bis(2-formyl-1*H*-pyrrole-3,4-dicarboxylate) (TEsbpyr-dial)

POCl$_3$ (450 μl, 4.8 mmol) was added slowly to DMF (380 μl, 4.8 mmol) taken in a flask and kept in an ice bath to form the Vilsmeier–Haack reagent. The reagent was dissolved in DCE, degassed and then added dropwise to another flask containing TEsbpyr (250 mg, 0.48 mmol) in DCE keeping the flask on ice bath in a N_2 atmosphere. The reaction mixture was degassed for 15 minutes and then refluxed for 5 hours. The reaction was monitored by TLC after charring the TLC plate using 2,4-DNP solution. The reaction was then quenched by adding a saturated solution of sodium acetate and worked up with dichloromethane. The organic layer was dried over Na_2SO_4, evaporated through a rotary-evaporator and purified by column chromatography on silica gel (100–200 mesh) with EtOAc: toluene (1 : 10). ^1H NMR(CDCl$_3$): δ (ppm) 1.21 (t, 6H), 1.39 (t, 6H), 4.15 (q, 4H), 4.40 (q, 4H), 6.72 (s, 1H), 7.01 (d, 2H), 7.26 (m, 5H), 9.92 (s, 2H), 11.35 (bs, 2H). ^{13}C {^1H} NMR (CDCl$_3$): δ (ppm) 13.97, 14.23, 29.63, 40.43, 114.19–139.67, 163.12, 164.87, 180.80. ESI-MS (positive ion mode, CH$_3$CN): 589.66 (75%, [M + Na]$^+$), 605.65 (25%, [M + K]$^+$), 567.65 (10%,[M + H]$^+$).

5-Phenyldipyrromethane

5-Phenyldipyrromethane was synthesized following the reported protocol.[79]

Tetraethylesterdiphenylporphyrin (TEsP)

TEsbpyr-dial (200 mg, 0.36 mmol) and 5-phenyldipyrromethane (79.5 mg, 0.36 mmol) were taken in a round bottom flask. Propionic acid (70 ml) was added and the system was refluxed for 30 minutes. The acid was distilled out from the reaction mixture. The solid product obtained was washed with warm water to remove the remaining acid. It was then dissolved in dichloromethane, dried over Na_2SO_4 and evaporated through a rotary-evaporator. Polypyrrole formed during the reaction was removed through column chromatography on silica gel (100–200 mesh) with EtOAc-hexane (1 : 4). The product was purified by a second column chromatography using 0.1% dichloromethane–methanol (99 : 1) mixture. ^1H NMR(CDCl$_3$): δ (ppm) −2.31 (br s, 1H), −2.05 (br s, 1H), 1.38 (t, 6H), 1.61 (t, 6H), 4.05 (t, 4H), 4.76 (q, 4H), 7.64–8.20 (m, 10H), 8.97 (d, 2H), 9.36 (d, 2H), 11.23 (s, 2H). ^{13}C {^1H} NMR (CDCl$_3$): δ (ppm) 13.92, 14.56,

22.83, 29.50, 29.84, 61.96, 62.10, 106.44, 119.45–141.19, 146.99, 151.09, 164.70, 166.85. ESI-MS (positive ion mode, CH_3CN): m/z 751.11 (50%, $[M + H]^+$).

FeTEsP

TEsP (30 mg, 0.04 mmol) was dissolved in dry THF (15 ml), 2,4,6-collidine (20.8 μl, 0.16 mmol) was added under a N_2 atmosphere to generate the porphyrin base. Then $FeBr_2$ (34.5 mg, 0.16 mmol) was added to it. The reaction mixture was stirred for 10 h at room temperature and the progress of the reaction was monitored by TLC. On full conversion, THF was evaporated using a rotary evaporator and workup was done using dichloromethane and HCl (to remove excess $FeBr_2$ as $FeCl_4^-$). The organic layer was dried over Na_2SO_4, evaporated through a rotary-evaporator and purified by column chromatography on silica gel (100–200 mesh) with 3.5% dichloromethane–methanol (96.5 : 3.5). ^1H NMR-paramagnetic (CDCl$_3$): δ (ppm) 75.99, 79.94, 81.83. ESI-MS (positive ion mode, CH_3CN): m/z 804.86 (100%, $[M]^+$).

ZnTEsP

TEsP (30 mg, 0.04 mmol) was dissolved in dry THF (15 ml). 2,4,6-Collidine (20.8 μl, 0.16 mmol) was added to generate the porphyrin base. Then $Zn(OAc)_2$ (29.35 mg, 0.16 mmol) was added to it. The reaction mixture was stirred for 10 h and the progress of the reaction was monitored by TLC. On full conversion, THF was evaporated and it was purified by column chromatography on silica gel (100–200 mesh) with 0.3% dichloromethane–methanol (99.7 : 0.3). ^1H NMR (CDCl$_3$): δ (ppm) −2.31.07 (t, 3H), 1.38 (t, 3H), 3.28 (q, 2H), 4.34 (q, 2H), 6.94–8.21 (m, 10H), 8.95 (d, 2H), 9.25 (d, 2H), 10.66 (s, 2H). ^{13}C $\{^1H\}$ NMR (CDCl$_3$): δ (ppm) 13.54, 14.42, 61.42, 61.70, 106.79, 119.79–144.89, 151.35, 153.86, 164.47, 167.10. ESI-MS (positive ion mode, CH_3CN): m/z 835.04 (100%, $[M + Na]^+$), 812.09 (80%, $[M]$).

Conflicts of interest

The authors declare no competing financial interests.

Acknowledgements

References

1 B. A. Averill, *Chem. Rev.*, 1996, **96**, 2951–2964.

2 L. B. Maia and J. J. G. Moura, *Chem. Rev.*, 2014, **114**, 5273–5357.

3 C. Moreno-Vivián, P. Cabello, M. Martínez-Luque, R. Blasco and F. Castillo, *J. Bacteriol.*, 1999, **181**, 6573.

4 O. Einsle, A. Messerschmidt, R. Huber, P. M. H. Kroneck and F. Neese, *J. Am. Chem. Soc.*, 2002, **124**, 11737–11745.

5 S. Rinaldo, G. Giardina, N. Castiglione, V. Stelitano and F. Cutruzzolà, *Biochem. Soc. Trans.*, 2011, **39**, 195.

6 Y. Shiro, *BBA, Biochim. Biophys. Acta, Bioenerg.*, 2012, **1817**, 1907–1913.

7 K. Brown, K. Djinovic-Carugo, T. Haltia, I. Cabrito, M. Saraste, J. G. Moura, I. Moura, M. Tegoni and C. Cambillau, *J. Biol. Chem.*, 2000, **275**, 41133–41136.

8 S. Teraguchi and T. C. Hollocher, *J. Biol. Chem.*, 1989, **264**, 1972–1979.

9 O. Einsle, A. Messerschmidt, R. Huber, P. M. H. Kroneck and F. Neese, *J. Am. Chem. Soc.*, 2002, **124**, 11737–11745.

10 S. J. George, J. W. A. Allen, S. J. Ferguson and R. N. F. Thorneley, *J. Biol. Chem.*, 2000, **275**, 33231–33237.

11 D. Bykov and F. Neese, *JBIC, J. Biol. Inorg. Chem.*, 2012, **17**, 741–760.

12 K. Kobayashi, A. Koppenhöfer, S. J. Ferguson, N. J. Watmough and S. Tagawa, *Biochemistry*, 2001, **40**, 8542–8547.

13 M. Radoul, D. Bykov, S. Rinaldo, F. Cutruzzolà, F. Neese and D. Goldfarb, *J. Am. Chem. Soc.*, 2011, **133**, 3043–3055.

14 S. Rinaldo, M. Brunori and F. Cutruzzolà, *Biochem. Biophys. Res. Commun.*, 2007, **363**, 662–666.

15 C. E. Cooper, *BBA, Biochim. Biophys. Acta, Bioenerg.*, 1999, **1411**, 290–309.

16 T. K. Das, E. K. Wilson, F. Cutruzzolà, M. Brunori and D. L. Rousseau, *Biochemistry*, 2001, **40**, 10774–10781.

17 X. J. Zhao, V. Sampath and W. S. Caughey, *Biochem. Biophys. Res. Commun.*, 1994, **204**, 537–543.

18 J. C. Maxwell and W. S. Caughey, *Biochemistry*, 1976, **15**, 388–396.

19 S. Rinaldo, K. A. Sam, N. Castiglione, V. Stelitano, A. Arcovito, M. Brunori, J. W. A. Allen, S. J. Ferguson and F. Cutruzzolà, *Biochem. J.*, 2011, **435**, 217.

20 J. S. Olson and G. N. Phillips, *J. Biol. Chem.*, 1996, **271**, 17593–17596.

21 M. Ikeda-Saito, Y. Dou, T. Yonetani, J. S. Olson, T. Li, R. Regan and Q. H. Gibson, *J. Biol. Chem.*, 1993, **268**, 6855–6857.

22 D. S. Bohle and C.-H. Hung, *J. Am. Chem. Soc.*, 1995, **117**, 9584–9585.

23 S. Amanullah, P. Saha, R. Saha and A. Dey, *Inorg. Chem.*, 2019, **58**, 152–164.

24 O. Einsle, P. Stach, A. Messerschmidt, J. Simon, A. Kröger, R. Huber and P. M. H. Kroneck, *J. Biol. Chem.*, 2000, **275**, 39608–39616.

25 D. Nurizzo, M.-C. Silvestrini, M. Mathieu, F. Cutruzzolà, D. Bourgeois, V. Fülöp, J. Hajdu, M. Brunori, M. Tegoni and C. Cambillau, *Structure*, 1997, **5**, 1157–1171.

26 M. G. Almeida, C. M. Silveira, B. Guigliarelli, P. Bertrand, J. J. G. Moura, I. Moura and C. Léger, *FEBS Lett.*, 2007, **581**, 284–288.

27 D. Bykov and F. Neese, *JBIC, J. Biol. Inorg. Chem.*, 2011, **16**, 417–430.

28 S. E. J. Bowman and K. L. Bren, *Nat. Prod. Rep.*, 2008, **25**, 1118–1130.

29 C. K. Chang and W. Wu, *J. Biol. Chem.*, 1986, **261**, 8593–8596.

30 A. M. Stolzenberg, S. H. Strauss and R. H. Holm, *J. Am. Chem. Soc.*, 1981, **103**, 4763–4778.

31 S. Ozawa, E. Sakamoto, Y. Watanabe and I. Morishima, *J. Chem. Soc., Chem. Commun.*, 1994, 935–936, DOI: 10.1039/C39940000935.

32 Y. Liu and M. D. Ryan, *Inorg. Chim. Acta*, 1994, **225**, 57–66.

33 Y. Liu, C. DeSilva and M. D. Ryan, *Inorg. Chim. Acta*, 1997, **258**, 247–255.

34 C. K. Chang, K. M. Barkigia, L. K. Hanson and J. Fajer, *J. Am. Chem. Soc.*, 1986, **108**, 1352–1354.

35 S. Ozawa, E. Sakamoto, T. Ichikawa, Y. Watanabe and I. Morishima, *Inorg. Chem.*, 1995, **34**, 6362–6370.

36 D. W. Feng, Y. S. Ting and M. D. Ryan, *Inorg. Chem.*, 1985, **24**, 612–617.

37 E. Fujita and J. Fajer, *J. Am. Chem. Soc.*, 1983, **105**, 6743–6745.

38 D. Lancon and K. M. Kadish, *J. Am. Chem. Soc.*, 1983, **105**, 5610–5617.

39 C. K. Chang and J. Fajer, *J. Am. Chem. Soc.*, 1980, **102**, 848–851.

40 M. H. Barley and T. J. Meyer, *J. Am. Chem. Soc.*, 1986, **108**, 5876–5885.

41 M. H. Rahman and M. D. Ryan, *Inorg. Chem.*, 2017, **56**, 3302–3309.

42 Y. Liu and M. D. Ryan, *J. Electroanal. Chem.*, 1994, **368**, 209–219.

43 I. K. Choi, Y. Liu, D. Feng, K. J. Paeng and M. D. Ryan, *Inorg. Chem.*, 1991, **30**, 1832–1839.

44 M. R. Kumar, D. Pervitsky, L. Chen, T. Poulos, S. Kundu, M. S. Hargrove, E. J. Rivera, A. Diaz, J. L. Colón and P. J. Farmer, *Biochemistry*, 2009, **48**, 5018–5025.

45 R. Lin and P. J. Farmer, *J. Am. Chem. Soc.*, 2000, **122**, 2393–2394.

46 L. E. Goodrich, S. Roy, E. E. Alp, J. Zhao, M. Y. Hu and N. Lehnert, *Inorg. Chem.*, 2013, **52**, 7766–7780.

47 C. K. Chang, *Biochemistry*, 1980, **19**, 1971–1976.

48 C.-B. Wang and C. K. Chang, *Synthesis*, 1979, **1979**, 548–549.

49 S. Amanullah, P. K. Das, S. Samanta and A. Dey, *Chem. Commun.*, 2015, **51**, 10010–10013.

50 J. K. Laha, S. Dhanalekshmi, M. Taniguchi, A. Ambroise and J. S. Lindsey, *Org. Process Res. Dev.*, 2003, **7**, 799–812.

51 L. W. Olson, D. Schaeper, D. Lancon and K. M. Kadish, *J. Am. Chem. Soc.*, 1982, **104**, 2042–2044.

52 L. A. Bottomley and K. M. Kadish, *Inorg. Chem.*, 1981, **20**, 1348–1357.

53 M. D. Bartberger, W. Liu, E. Ford, K. M. Miranda, C. Switzer, J. M. Fukuto, P. J. Farmer, D. A. Wink and K. N. Houk, *Proc. Natl. Acad. Sci. U.S.A*, 2002, **99**, 10958.

54 J. Pellegrino, S. E. Bari, D. E. Bikiel and F. Doctorovich, *J. Am. Chem. Soc.*, 2010, **132**, 989–995.

55 L. E. Goodrich, F. Paulat, V. K. K. Praneeth and N. Lehnert, *Inorg. Chem.*, 2010, **49**, 6293–6316.

56 A. P. Hunt and N. Lehnert, *Acc. Chem. Res.*, 2015, **48**, 2117–2125.

57 K. M. Vogel, P. M. Kozlowski, M. Z. Zgierski and T. G. Spiro, *J. Am. Chem. Soc.*, 1999, **121**, 9915–9921.

58 C. M. Coyle, K. M. Vogel, T. S. Rush, P. M. Kozlowski, R. Williams, T. G. Spiro, Y. Dou, M. Ikeda-Saito, J. S. Olson and M. Z. Zgierski, *Biochemistry*, 2003, **42**, 10342.

59 S. Rinaldo, A. Arcovito, M. Brunori and F. Cutruzzolà, *J. Biol. Chem.*, 2007, **282**, 14761–14767.

60 A. L. Speelman and N. Lehnert, *Acc. Chem. Res.*, 2014, **47**, 1106–1116.

61 Z. Wei and M. D. Ryan, *Inorg. Chem.*, 2010, **49**, 6948–6954.

62 A. E. Servid, A. L. McKay, C. A. Davis, E. M. Garton, A. Manole, P. S. Dobbin, M. A. Hough and C. R. Andrew, *Biochemistry*, 2015, **54**, 3320–3327.

63 J. J. Warren, T. A. Tronic and J. M. Mayer, *Chem. Rev.*, 2010, **110**, 6961–7001.

64 D. D. M. Wayner and V. D. Parker, *Acc. Chem. Res.*, 1993, **26**, 287–294.

65 V. Shafirovich and S. V. Lymar, *Proc. Natl. Acad. Sci. U.S.A*, 2002, **99**, 7340.

66 M. A. Rhine, A. V. Rodrigues, R. J. B. Urbauer, J. L. Urbauer, T. L. Stemmler and T. C. Harrop, *J. Am. Chem. Soc.*, 2014, **136**, 12560–12563.

67 M. Ali, N. Stein, Y. Mao, S. Shahid, M. Schmidt, B. Bennett and A. A. Pacheco, *J. Am. Chem. Soc.*, 2019, **141**, 13358–13371.

68 M. C. Silvestrini, M. G. Tordi, G. Musci and M. Brunori, *J. Biol. Chem.*, 1990, **265**, 11783–11787.

69 T. Vangberg and A. Ghosh, *J. Am. Chem. Soc.*, 1999, **121**, 12154–12160.

70 W. R. Scheidt, H. F. Duval, T. J. Neal and M. K. Ellison, *J. Am. Chem. Soc.*, 2000, **122**, 4651–4659.

71 E. G. Abucayon, R. L. Khade, D. R. Powell, Y. Zhang and G. B. Richter-Addo, *J. Am. Chem. Soc.*, 2016, **138**, 104–107.

72 E. G. Abucayon, R. L. Khade, D. R. Powell, M. J. Shaw, Y. Zhang and G. B. Richter-Addo, *Dalton Trans.*, 2016, **45**, 18259–18266.

73 N. G. Connelly, P. T. Draggett, M. Green and T. A. Kuc, *J. Chem. Soc., Dalton Trans.*, 1977, 70–73, DOI: 10.1039/DT9770000070.

74 T. C. Harrop, Z. J. Tonzetich, E. Reisner and S. J. Lippard, *J. Am. Chem. Soc.*, 2008, **130**, 15602–15610.

75 M. J. Frisch, *Version C.02*, Gaussian, Inc., 2004.

76 R. Krishnan, J. S. Binkley, R. Seeger and J. A. Pople, *J. Chem. Phys.*, 1980, **72**, 650–654.

77 A. D. McLean and G. S. Chandler, *J. Chem. Phys.*, 1980, **72**, 5639–5648.

78 M. Cossi, N. Rega, G. Scalmani and V. Barone, *J. Comput. Chem.*, 2003, **24**, 669–681.

79 B. J. Littler, M. A. Miller, C.-H. Hung, R. W. Wagner, D. F. O'Shea, P. D. Boyle and J. S. Lindsey, *J. Org. Chem*, 1999, **64**, 1391–1396.